Graphene Plasmons in Triangular Wedges and Grooves

Gonçalves, P. A. D.; Dias, E. J. C.; Xiao, Sanshui ; Vasilevskiy, M. I.; Mortensen, N. Asger; Peres, N. M. R.

Published in:
A C S Photonics

Link to article, DOI:
10.1021/acsphotonics.6b00674

Publication date:
2016

Document Version
Peer reviewed version

Graphene Plasmons in Triangular Wedges and Grooves

P. A. D. Gonçalves,[*,†,‡] E. J. C. Dias,[¶] Sanshui Xiao,[†,‡] M. I. Vasilevskiy,[¶] N. Asger Mortensen,[†,‡] and N. M. R. Peres[*,¶]

†*Department of Photonics Engineering, Technical University of Denmark, DK-2800 Kgs. Lyngby, Denmark*

‡*Center for Nanostructured Graphene, Technical University of Denmark, DK-2800 Kgs. Lyngby, Denmark*

¶*Department of Physics and Center of Physics, University of Minho, PT-4710–057, Braga, Portugal*

E-mail: padgo@fotonik.dtu.dk; peres@fisica.uminho.pt

Abstract

The ability to effectively guide electromagnetic radiation below the diffraction limit is of the utmost importance in the prospect of all-optical plasmonic circuitry. Here, we propose an alternative solution to conventional metal-based plasmonics by exploiting the deep subwavelength confinement and tunability of graphene plasmons guided along the apex of a graphene-covered dielectric wedge or groove. In particular, we present a quasi-analytic model to describe the plasmonic eigenmodes in such a system, including the complete determination of their spectrum and corresponding induced potential and electric field distributions. We have found that the dispersion of wedge/groove graphene plasmons follows the same functional dependence as their flat-graphene plasmons counterparts, but now scaled by a (purely) geometric factor in which all the information

about the system's geometry is contained. We believe our results pave the way for the development of novel custom-tailored photonic devices for subwavelength waveguiding and localization of light based on recently discovered 2D materials.

Keywords

graphene plasmons, plasmonics, nanophotonics, channel plasmons, wedge, groove

Over the last couple of decades we have been witnessing a steady, exponential growth in the amount of information produced on a daily basis. In today's "information age", huge amounts of data must be processed, stored, and delivered around the world. While the data-processing part is still primarily carried by electronics, the routing of large volumes of information is handled with photonic technologies since only these can meet the requirements in terms of high-speed, density and bandwidth. One of the greatest ambitions of modern nanophotonics[1] is to bridge the gap between electronic and photonic components, and ultimately to replace electronic circuits and processing units by their photonic-based counterparts. Current scalable photonic-based communications, however, still could not surpass the threshold towards miniaturization posed by the diffraction limit. In this regard, a great deal of hope[2] has been deposited in the sub-discipline of photonics known as plasmonics,[3,4] which exploits the ability of surface plasmon-polaritons (SPPs)—collective oscillations of the free-electrons at metal/dielectric interfaces—to localize light into subwavelength dimensions.[5–8] Although the pursuit of plasmonic devices suitable for mass-production is still going on, plasmonics has already achieved some milestones, for instance, subwavelength plasmonic circuitry including waveguides, interferometers and resonators,[9–12] nanolasers,[13–16] quantum optics with or mediated by SPPs,[17–21] label-free and single molecule biochemical sensing,[22–26] high-resolution nanoscopy,[27,28] and even cancer theranostics.[29–31]

A key component in any plasmonic circuit would be an element to transfer and guide the electromagnetic (EM) fields from point A to point B. Typical SPP-guiding struc-

tures[32] consist in small metallic stripes on a dielectric substrate,[3,32] chains of plasmonic nanoparticles,[33–35] metal/dielectric/metal slabs,[32] or V-shaped grooves carved into a metallic substrate,[36–38] just to name a few. Among these, the latter are believed to be appealing candidates for subwavelength waveguiding of light since they support SPP modes coined as channel plasmon-polaritons (CPPs),[3,36] which have been shown to deliver localized EM fields with relatively long propagation lengths,[12,36,39] ability to work at telecommunication wavelengths,[10,40,41] and feasibility to steer the EM field along bends.[10,42] The earliest reference on CPPs can be found in a theoretical investigation carried out by Dobrzynski and Maradudin, having obtained analytic expressions in the electrostatic limit for an infinitely sharp wedge.[43] Many subsequent works then followed in similar wedge configurations with a rounded edge.[44–47] During the past decade—owing to the rapid progresses in nanofabrication and computational tools—a renewed interest has emerged on CPPs guided along triangular grooves sculpted in metal substrates, leading to a plethora of theoretical and experimental studies.[36,38,40,48–51].

In recent years, graphene[52,53]—an atomically-thin sp^2-hybridized carbon allotrope in which the atoms sit at the vertexes of a honeycomb lattice—has come to the light as a novel plasmonic material.[54–58] Graphene is classified as a two-dimensional (2D) semi-metal whose charge-carriers exhibit a linear dispersion.[52,53] When doped, graphene also sustains plasmon-polaritons that inherit the extraordinary optoelectronic properties of this material. In particular, gate-tunable graphene surface plasmons (GSPs) have been shown to deliver highly confined EM fields into deep subwavelength regions, large field-enhancements, strong light-matter interactions, and carry the prospect of low-loss plasmonics.[54–59] In addition, the ability to easily control the carrier-density in graphene, e.g. by electrostatic gating and/or chemical means, constitutes a major advantage of GSPs over conventional metal-based plasmonics. Popular configurations to realize GSPs involve the nanostructuring of an otherwise continuous graphene sheet into graphene ribbons,[26,60–63] disks,[64–68] rings,[64,65] and graphene anti-dots (either as individual structures or in periodic arrays).[67,69,70]

Here, we propose a different approach to deliver strongly localized GSPs which does not involve any nanopatterning done on the graphene layer; it simply consists in depositing graphene onto a V-shaped wedge or groove previously sculpted in the receiving substrate (a different, but related configuration was the subject of a previous numerical study[71]). This can be done by employing the same techniques used to fabricate metallic grooves,[36] followed by the graphene deposition or even direct-growth on a pre-configured copper substrate.[72] Other possibilities include folding a graphene layer or by exploring the formation of wrinkles (either naturally occuring[73–75] or deliberately formed[72]). In this way, one departures from customary flat-graphene geometries and effectively produces a 1D channel which not only confines light in the vertical direction that bisects the channel, but is also capable of producing lateral confinement of EM radiation.

In this work, we present a quasi-analytic method to derive the dispersion relation and corresponding spatial distributions of the potential and electric fields akin to GSPs guided along a V-shaped channel. We shall consider both the wedge and groove geometries—see Fig. 1. In what follows we work within the electrostatic limit, which turns out to be a very good approximation for GSPs owing to the large wavevectors carried by plasmons in graphene (and thus retardation becomes unimportant). Interestingly, we find that for a fixed wedge/groove angle the corresponding wedge/groove graphene plasmon (WGP/GGP) dispersions follow a universal scaling law that depends purely on the system's geometry. Thus, by performing the calculations for a given angle, φ, one immediately gains complete knowledge of the WGPs/GGPs' wavevectors for every frequency—in other words, all the modes and corresponding dispersion relations are obtained at once. This constitutes an enormous advantage in terms of computational resources and time when gauged against full-wave numerical simulations. From a device-engineering perspective this scaling property should also significantly ease design of waveguides for given applications. Finally, in further support of the accuracy of our quasi-analytic technique, we have also performed rigorous electrodynamic simulations with the aid of a commercially available (Comsol MultiPhysics)

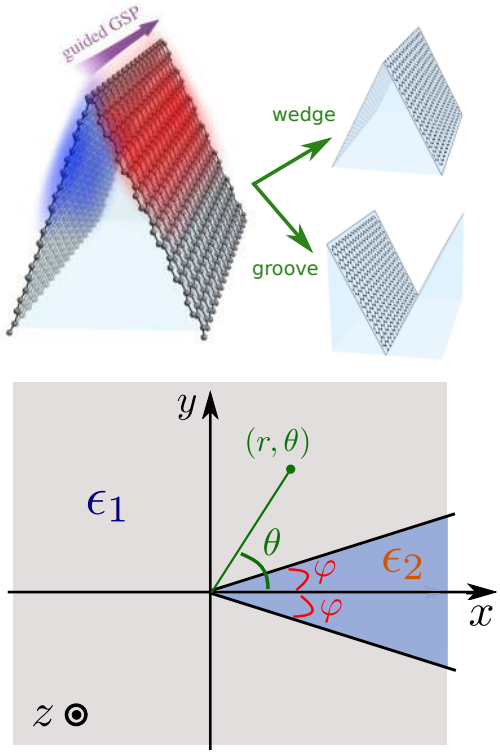

Figure 1: Upper panel: pictorial representation of a guided GSP mode along a dielectric wedge; we denote the system a *wedge* (*groove*) whenever the medium filling the 2φ-open region possesses a higher (lower) value for the relative permittivity. Lower panel: coordinate system for a wedge or groove interface—with an opening angle of 2φ— between two dielectric media characterized by relative permittivities ϵ_2 (for $-\varphi \leq \theta \leq \varphi$) and ϵ_1 (for $\varphi \leq \theta \leq 2\pi - \varphi$).

finite-element method (FEM), to which we have obtained a remarkable agreement.

We demonstrate that by using graphene-covered triangular wedges or grooves one can harness the unique properties of GSPs to create novel 1D subwavelength plasmonic waveguides that can squeeze light into deep subwavelength regimes. This becomes particularly relevant at THz and mid-IR frequencies since traditional metal-based plasmonics perform poorly in this spectral range (resembling freely propagating light).[3] Furthermore, we believe that this work can set the stage for future investigations of graphene plasmons in 1D channels, with potentially relevant applications ranging from plasmonic circuitry and waveguiding to biochemical sensing with WGPs/GGPs or their integration with microfluidics on a chip.

Results and Discussion

We consider an idealized geometry in which a graphene monolayer is sandwiched between a triangular dielectric wedge (or groove) with relative permittivity ϵ_2 and a capping dielectric material with relative permittivity ϵ_1, as depicted in Fig. 1. As it will become apparent later, our model is completely general irrespective of the specific values for the dielectric constants of the cladding insulators. However, in order to cope with the standard nomenclature, we shall refer to a *wedge* whenever $\epsilon_2 > \epsilon_1$ and vice-versa to denote a *groove*. In addition, albeit here we are primarily interested in graphene, the theory outlined below can be applied to any 2D layer deposited onto the triangular shape, be it a 2D electron gas or a doped 2D transition metal dichalcogenide (TMDC), etc.

Before proceeding to the description of our quasi-analytic method, we first bring to the reader's attention that one can treat the cases of even and odd symmetry in the potential (or induced charges) — with respect to the line bisecting the triangular cross-section— separately, as this makes the problem more amenable to handle. In particular, for the case of even symmetry (i.e., when the induced charges are symmetric in the graphene half-planes which constitute the V-shape), we have found that these even-symmetry modes are not highly confined near the apex of the wedge/groove, with their dispersion being virtually the same as for GSPs in a flat, planar dielectric/graphene/dielectric interface (cf. SI). Conversely, as it will become clear ahead, the corresponding odd WGPs/GGPs modes exhibit strong field confinement near the apex of the wedge/groove, and therefore we shall limit our discussion solely to the odd-symmetry case hereafter. Owing to the high localization of the field near the apex, we note that although we assume (for simplicity) an infinitely long V-shape, the theory developed here remains adequate in the description of V-structures of finite height/depth as long as their size is larger than the region spanned by the field distribution along the axis of symmetry.

The extremely large wavevectors (when compared with light's free-space wavevector, $k_0 = \omega/c$) attained by graphene plasmons allow us to treat plasmonic excitations in graphene

within the electrostatic limit with high accuracy. In this regime, the induced electric potential akin to GSPs must satisfy Poisson's equation, which in cylindric coordinates reads

$$\left[\frac{\partial^2}{\partial r^2}+\frac{1}{r}\frac{\partial}{\partial r}+\frac{1}{\partial r^2}\frac{\partial^2}{\partial \theta^2}-q^2\right]\Phi(r,\theta)=-\frac{\rho(r,\theta)}{\epsilon_0}\ , \tag{1}$$

where we have written the scalar potential as $\Phi(\mathbf{r}) = \Phi(r,\theta)e^{iqz}$, owing to the system's translational invariance along the z-axis (an implicit time-dependence of the form $e^{-i\omega t}$ is assumed). This effectively reduces our initial 3D problem into a 2D one, and will allow us to parameterize the dispersion relation of the guided GSPs in terms of the propagation constant q, i.e. $\omega \equiv \omega(q)$. Hence, the solution of Eq. (1) renders the WGPs/GGPs modes which propagate along the longitudinal direction. Formally, the solution of this equation in the medium $j = 1, 2$ can be written as

$$\Phi(r,\theta)=\frac{i\sigma(\omega)}{\omega}\int_0^\infty dr' G_j(r,\theta;r',\varphi)\left[\frac{\partial^2}{\partial r'^2}-q^2\right]\Phi(r',\varphi)\ , \tag{2}$$

where $\sigma(\omega)$ is the dynamical conductivity of graphene, and $G_j(r,\theta;r',\varphi)$ is the Green's function associated with Eq. (1) in that medium; the latter is defined explicitly in the SI. Moreover, when writing the preceding equation, we have expressed the carrier-density as $\rho(r,\theta) = -en(r)\delta(\theta-\varphi)/r$, where the 2D particle density, $n(r)$, was written in terms of the electrostatic potential by combining the continuity equation together with Ohm's law (cf. SI). We further remark that we only need to solve for the potential in, say, the upper-half space ($0 \leq \theta \leq \pi$), since we are looking for solutions in which the potential is odd with respect to the symmetry axis. It is clear from Eq. (2) that the potential in the *whole space* can only be derived once the potential *at the graphene sheet* (i.e., $\theta = \varphi$) is determined. To that end, we set $\theta = \varphi$ and then employ an orthogonal polynomials expansion technique[54,76,77] to transform the above integro-differential equation for the potential at the graphene, $\phi(r) \equiv \Phi(r,\varphi)$, into a standard linear algebra eigenproblem. This is done by expanding the electrostatic potential evaluated at the graphene layer as $\phi(r) = \sum_n c_n L_n^{(0)}(qr)e^{-qr/2}$, with $L_n^{(0)}$ denoting

the generalized Laguerre polynomials,[78] and where the c_n's are the entries of the eigenvectors defined by the following eigensystem (obtained by exploiting the appropriate orthogonality relations[78]):

$$\frac{i\omega}{q\sigma(\omega)}c_m = \sum_{n=0}^{\infty} U_{mn}c_n \ , \tag{3}$$

where the matrix elements U_{mn} read

$$U_{mn} = \int_0^\infty \int_0^\infty dxdy \ G(x,\varphi;y,\varphi)e^{-\frac{x+y}{2}}L_m^{(0)}(x) \\ \times \left[\frac{3}{4}L_n^{(0)}(y) - L_{n-2}^{(2)}(y) - L_{n-1}^{(1)}(y)\right] \ . \tag{4}$$

We note that the double integration over the dimensionless variables $x = qr$ and $y = qr'$ can be performed analytically, thereby making the computation of the matrix elements extremely fast. Notice that we have dropped the index j in the Green's function because the boundary condition at $\theta = \varphi$ enforces that $G_1(x,\varphi;y,\varphi) = G_2(x,\varphi;y,\varphi)$, and therefore one can choose either Green's function arbitrarily without any loss of generality.

The eigenvalue equation (3) can be solved numerically using standard linear-algebra routines. Once we find the corresponding eigenvalues $\tilde{\lambda}_n$ (whose number matches the length of the vector $\vec{c}$, i.e. $N+1$, where N truncates the expansion for $\phi(r)$, and convergence was checked empirically—cf. SI), the spectrum of graphene plasmons traveling along the triangular wedge/groove straightforwardly follows from

$$\frac{i\omega}{q\sigma(\omega)} = \tilde{\lambda}_n \ , \tag{5}$$

where, for a given opening angle 2φ, Eq. (5) returns a discrete set of WGPs/GGPs modes. We stress that all the momentum and frequency dependence stems from the LHS of the previous equation; hence, the eigenvalues $\tilde{\lambda}_n \equiv \tilde{\lambda}_n(\varphi)$ carry a purely geometric meaning since they depend uniquely on the configuration of the system (opening angle and material parameters). In particular, using graphene's Drude-like conductivity with negligible damping,[54]

one obtains a "universal scaling law" for the dispersion relation of wedge/groove graphene plasmons,

$$\Omega(q) = \Omega_{\text{flat}}(q)\frac{2}{\pi}\sqrt{\lambda_n}\ , \tag{6}$$

where the relation $\tilde{\lambda}_n = \frac{4}{\pi^2\epsilon_0(\epsilon_1+\epsilon_2)}\lambda_n$ has been used, and stems from factorizing a constant proportionality factor entering in the Green's function (see the text after Eq. (S33) in the SI). The above equation gives the energy of the guided graphene plasmon modes parameterized by the propagation constant along the apex of the wedge. Here, $\Omega_{\text{flat}}(q) = \sqrt{\frac{4\alpha\hbar c}{\epsilon_1+\epsilon_2}E_F q}$ is simply the dispersion relation followed by GSPs in flat graphene[54] sandwiched between two dielectrics with ϵ_1 and ϵ_2 (where $\alpha \simeq 1/137$ denotes the fine-structure constant). Notice that once we have determined λ_n, we possess complete knowledge of the WGPs/GGPs spectrum—for any point in the entire (q,ω)-space —, all of this with only *one* computation. In fact, we can even plot the dispersion of distinct 2D materials that support SPPs modes from a single computation of λ_n, since the latter does not depend on the 2D conductivity that characterizes the particular 2D material [recall Eq. (5)]. It is instructive to note that, in general, the spectrum of WGPs/GGPs contains a discrete set of even and odd modes (although here we describe only modes with odd-symmetry for the reason stated above in the text), in a similar way to SPPs supported at metallic wedges/grooves.[36] This is a consequence of the lateral confinement near the tip of the wedge (or the bottom of the groove), and bears some resemblance to finding the electronic eigenstates of a particle in a quantum wire.[79]

In Fig. 2 we have plotted the dispersion relation of graphene plasmons guided along the edge of triangular wedges and grooves with different opening angles, 2φ (indicated in the insets), which, as we have already anticipated, consists in a discrete set of well-defined modes with increasing energy. The figure plainly shows that the spectrum of both WGPs and GGPs strongly depend on the angles of the triangular opening, with smaller angles rendering correspondingly larger plasmon wavevectors for the same frequency, which in turn is an indication of stronger field confinement near the apex of the V-shape. Another striking feature visible in the figure is the outstanding agreement between the quasi-analytic theory detailed

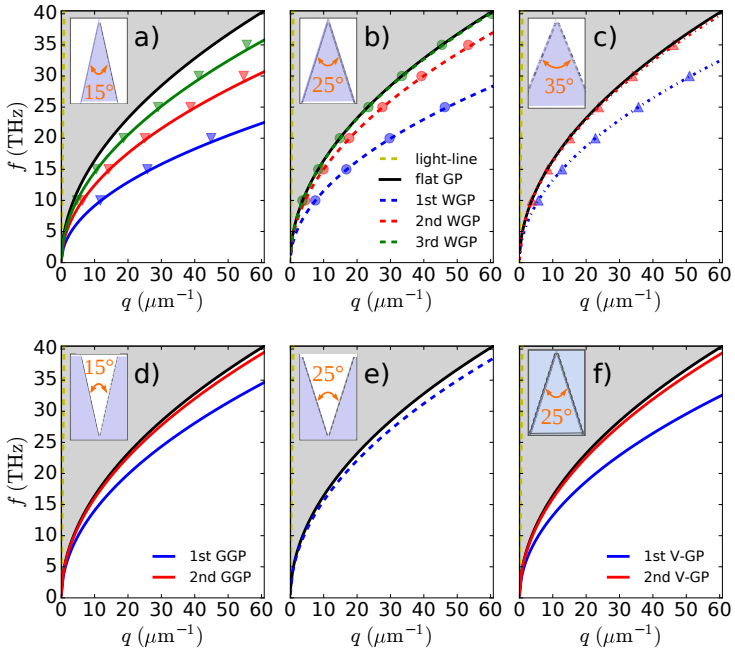

Figure 2: Spectrum of WGPs (upper row) and GGPs (first two bottom panels) sustained in different graphene-covered triangular configurations, with different opening angles, 2φ (indicated in the insets), as given by Eq. 6 [we take $E_F = 0.4$ eV]. The solid black line represents the dispersion of GSPs in a flat interface and serves as reference. The colored $\bigtriangledown$, $\bigcirc$ and $\bigtriangleup$ data points figuring in the upper row correspond to the results for the WGP dispersion as obtained from full-wave numerical simulations (COMSOL's finite-element method). The insets' shading ▭ represents an insulator with $\epsilon = 4$, whereas the white regions denote a medium with $\epsilon = 1$ (e.g. air). The last panel shows the spectrum of GSPs guided along a V-shaped graphene embedded in a homogeneous medium with $\epsilon = 2.5$ (shaded in the inset as ▭).

above and the electrodynamic simulations using the FEM technique (see SI for details on the simulations). This constitutes further evidence of the ability of our quasi-analytic method to render accurate results, while also providing a deeper fundamental understanding of the scaling properties. Also from the inspection of Fig. 2, a strong contrast can be perceived between the dispersion curves akin to WGPs and GGPs, demonstrating the superiority of the former in squeezing light below the diffraction limit as they attain larger wavevectors for the same angle of the structure. We further note that one can transform a wedge into a groove and vice-versa either by swapping the values of ϵ or by applying the angular transformation $\varphi \to \pi - \varphi$ (this essentially interchanges the Green's functions G_1 and G_2). For the sake of completeness, in Fig. 2f panel we have portrayed the spectrum of GSPs guided along a triangular apex embedded in a homogeneous dielectric medium with the same average relative permittivity as its wedge and groove counterparts. It can be observed that—for the same angle—each of the modes attain increasingly larger wavevectors as we move from a groove, embedded and wedge configuration (in this order). This hints us that the ability to reach deep subwavelength regimes strongly depends on the ϵ_2/ϵ_1 ratio, for a fixed (acute) angle. Such prediction is confirmed by Fig. 3, in which we observe that the scaling factor appearing in Eq. (6) decreases monotonically with increasing ϵ_2/ϵ_1. In turn, this translates into higher effective indexes, $n_{\text{eff}} = q/k_0$, for larger quotients ϵ_2/ϵ_1. As an example, we have obtained $n_{\text{eff}} \simeq 72$ for a frequency of 20 THz in a configuration corresponding to panel in Fig. 2b. Even larger effective indexes can be obtained at higher frequencies (for instance, for the CO_2 laser wavelength of $10.6\,\mu$m this value climbs to $n_{\text{eff}} \simeq 100$, using the same parameters). Naturally, the higher amount of field localization promoted by the WGP/GPP modes comes hand in hand with slightly larger propagation losses (cf. SI), a trait that is well-known and characteristic of plasmonics. Still, we have found that the number of plasmon oscillations within a propagation length[4,54] remains unaltered when comparing between different mode orders or flat-GSPs (see SI for further details). Indeed, owing to the "universal scaling" epitomized by Eqs. (5) and (6), the *ratio* between loss and field confinement is independent

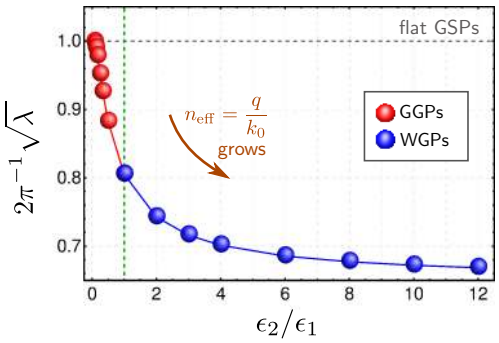

Figure 3: Dependence of the eigenvalues akin to the fundamental mode—in fact, of the proportionality factor, $2\pi^{-1}\sqrt{\lambda}$, figuring in Eq. (6)—as a function of the ratio ϵ_2/ϵ_1. In computing the data in blue we have fixed $\epsilon_1 = 1$ while varying ϵ_2, and vice-versa for the red data points. The vertical green dashed line indicates the point where $\epsilon_1 = \epsilon_2 = 1$, whereas the horizontal gray dashed line sets the upper bound corresponding to the flat GSP dispersion. We further note that the value of λ is also sensitive to the absolute value of the dielectric constant that is kept constant while the other varies.

of the mode order and is the same as for flat-GSPs.

Before concluding the analysis of Fig. 2, we highlight the capability of these guided GSPs modes to render extreme light-localization. This ability can be appreciated by considering the distance of their dispersion curves to the light-line (yellowish dashed-line near the vertical axis) and the large effective indexes that were obtained. This departure from the light-cone also justifies the high accuracy in the treatment of these modes within the electrostatic limit, as retardation effects are negligible and GSPs possess an essentially electrostatic character.

Potential and electric-field distributions. Furthermore, we remark that the solution of the eigenproblem in Eq. (3) also allows us to reconstruct the electrostatic potential within the graphene by feeding the obtained eigenvalues and eigenvectors back into the expansion for $\phi(r)$. From here, the 2D particle-density directly follows via $n(r) = \frac{\sigma(\omega)}{ie\omega}\left[\partial^2/\partial r^2 - q^2\right]\phi(r)$ (see SI). Both these physical quantities, evaluated at the graphene's surface, that is $\theta = \varphi$ (at $\theta = -\varphi$ the distributions are antisymmetric), are shown in Fig. 4. Here, we consider WGPs with frequency $f = 20$ THz guided along a $2\varphi = 25°$ triangular wedge (which corresponds to the case illustrated in Fig. 2b).

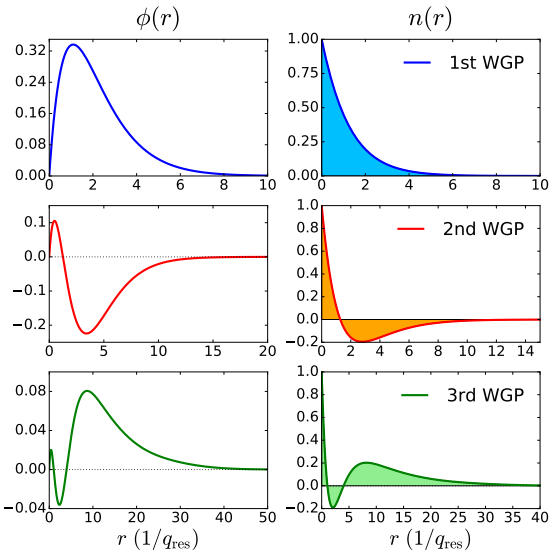

Figure 4: Radial distributions of the electrostatic potential, $\phi(r) \equiv \Phi(r, \varphi)$, and 2D particle density, $n(r)$, for the three lowest eigenmodes of a 25° wedge covered with graphene (in a.u.), at a resonant frequency of $f = 20$ THz. The radial coordinate is plotted in units of the inverse wavevector akin to each mode [obtained by inverting Eq. (6) for a angular frequency of $\omega = 2\pi \times 20$ THz]. The remaining parameters are the same as in Fig. 2b (i.e., $\epsilon_1 = 1$, $\epsilon_2 = 4$, and $E_F = 0.4$ eV).

Figure 4 indicates that the highest density of charge-carriers occurs at the apex of the wedge, irrespective of the mode order, although the density drops towards zero at increasingly larger distances from the origin for the higher-order modes. In addition, we note that $q_{3\mathrm{rd}}^{-1} > q_{2\mathrm{nd}}^{-1} > q_{1\mathrm{st}}^{-1}$ for the same frequency, which makes the difference in the confinement even more dramatic. We emphasize that the number of nodes of both $\phi(r)$ and $n(r)$ is given by $m - 1$, where $m = 1, 2, ...$ (for modes below the flat GSP dispersion curve) stands for the mode order. On the other hand, the value of the potential evaluated at the graphene layer is large *near* the vertex of the triangular cross-section, specially for the fundamental mode (where it is maximum). We acknowledge that, however, it is not located *exactly* at $r = 0$. This is consequence of the infinitely sharp apex, whose corresponding Green's functions strongly oscillate at very small r, since they are not well-defined (but are bounded, i.e. do not diverge) in the $r \to 0$ limit. Conversely, for modes with higher energy, the potential tends to shift its weight farther from the apex of the V-structure as the mode order increases. Such behavior

was already expected in the light of Fig. 2, since the WGP wavelength becomes smaller as the mode order decreases; as a consequence, the fundamental WGP mode exhibits the highest field-confinement, thereby being able to probe deeper into the V-wedge owing to its shorter wavelength when compared to the higher branches of the polaritonic spectrum. Again, we stress that although our model assumes infinitely deep triangular cross-sections, it can accurately describe finite-sized V-shapes as long as the height (depth) of the wedge (groove) is located at a distance somewhere along the "tail" of the quantities plotted in Fig. 4 (where they are essentially zero). In passing, we note that apart from the plasmon modes located at the apex of, say, a wedge (2φ opening angle), the modes sustained at the corresponding "grooves", originating from the truncation of the structure—forming a $\pi/2+\varphi$ angle—, can also be determined using the same guidelines as above, provided that the height of the wedge is large enough to prevent the hybridization of the modes. The same reasoning also holds for grooves.

We recall that once in possession of the potential evaluated at the graphene, one can build the potential in the entire coordinate space using Eq. (2). From here, the corresponding induced electric field follows directly by taking the gradient, i.e. $\mathbf{E}(\mathbf{r}) = -\nabla\Phi(\mathbf{r})$. In what follows, we shall discuss only the spatial distributions of the potential and electric field within the plane transverse to the propagation direction, since its dependence along the z-axis is trivial due to the translational invariance of the system along this direction. The calculated 2D distributions (in the xy-plane) of the potential and concomitant electric field akin to WGPs in a representative $2\varphi = 25^\circ$ dielectric wedge are shown Fig. 5. Note that the electric field in cartesian coordinates can be fetched from its polar version by applying a rotation matrix, namely $(E_x, E_y)^T = R(\varphi)(E_r, E_\theta)^T$. The figure exhibits telling evidence of the remarkable confinement WGP are able to attain near the apex of the wedge (the results for the groove are qualitatively similar, albeit with slightly less localization for the same resonant frequency); this can be observed both from the induced potential or the electric-field. The intensity plot in the background of the vectorial representation of the 2D $\mathbf{E}(x, y)$

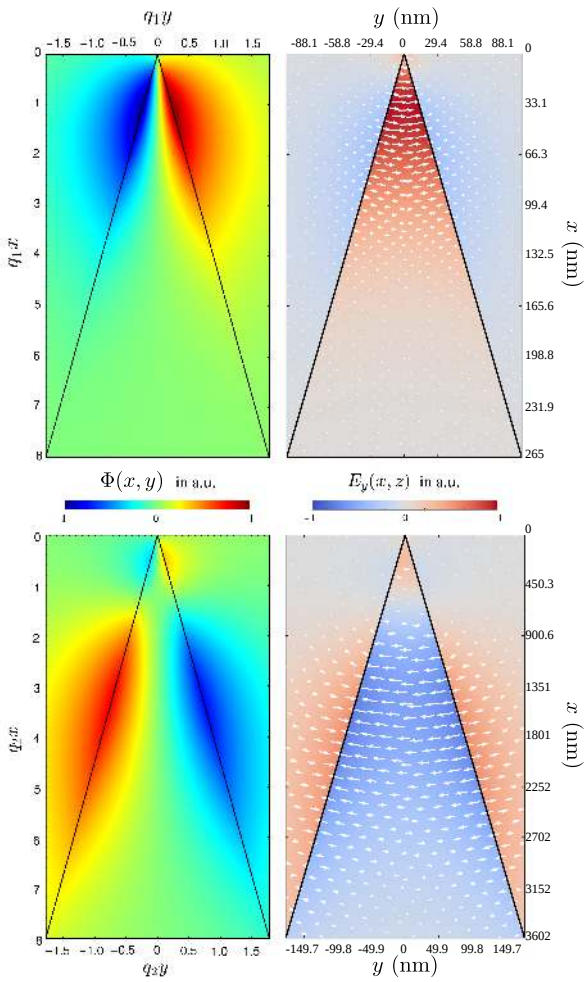

Figure 5: Two-dimensional potential, $\Phi(x, y)$, and electric-field distributions, $\mathbf{E}(x, y) = -\nabla_{2D}\Phi(x, y)$, ascribed to the fundamental (upper panels) and second order (lower panels) WGPs modes, at a resonant frequency of $f = 20$ THz. The parameters used in these computations match the ones in Fig. 4. The plotted region is the same in each pair of 2D plots, with axes of the panels on the left written in dimensionless units (normalized to the corresponding propagation constants) and the axes of the plots on the right are given in nanometers.

refers to the value of the y-component of this quantity, which is dominant in most of the spatial region. Notice that since the potential has odd symmetry with relation to the $y = 0$ plane, then the correspondent component of the electric field must be of even symmetry. It should also be highlighted that the vertical confinement (with respect to the apex edge) decreases rather rapidly as we move from the fundamental resonance to the higher order branches of the polaritonic spectrum. For the particular case depicted in the figure, the

lowest energy mode essentially remains localized within the first 200 nm, whereas for the second order mode that distance grows beyond 3.6 μm. Figure 5 also serves to support our previous claim that despite inherent simplifications in our theory, it may still be applied to realistic wedges (grooves) of finite height (depth). More specifically, the results portrayed in the figure accurately describe the 1st WGP in a 200nm-tall dielectric wedge, or, instead, *both* WGPs modes in a wedge with about 4 μm in height.

The behavior of the spatial distributions displayed in Fig. 5 is qualitatively maintained throughout most of the dispersion curve (and similarly for different angles), the only important difference being the degree of confinement in the whereabouts of the apex edge. Therefore, an infinitely vast number of V-shaped geometric configurations, with different angles, heights or depths, may be engineered depending on the required level of localization and/or frequency region of interest. In this regard, one can use our model to effectively design and architecture a device which meets the pre-established requirements in terms of operating frequency range and dimensions.

Concluding Remarks and Outlook

In summary, we envision the exploitation of the folding of an otherwise planar graphene sheet—or any other SPP-supporting 2D material—into an (out-of-plane) triangular-like shape as a mean to achieve deep subwavelength waveguiding and light-localization using the plasmon modes guided along the apex of a V-shaped substrate. The fabrication of such devices is well within reach of current experimental state-of-the-art capabilities, as much of the technology has already been developed in the context of traditional 3D metal plasmonics. As an example, nanoimprint approaches developed for metal grooves[80] could be readily applied also to the present case. The same goes in what concerns potential mechanisms to excite these modes, since the same techniques used to excite CPPs could also be applied to excite WGP/GGP modes (e.g. end-fire coupling or excitation by fast electrons).[36] In

this article, we have outlined a quasi-analytic method to theoretically describe graphene plasmons either guided along the ridge of a dielectric wedge or along the valley of a groove carved in an insulating substrate. The model accurately obtains the spectrum of the plasmonic eigenmodes supported by the aforementioned structures, as well as the potential and electric field distributions akin to those excitations. The computed modal distributions advocate the ability of these modes to achieve large field-enhancements and to deliver strong light-localization in the neighborhood of the triangular edge. Interestingly, we have found that the dispersion of each particular WGP/GGP mode obeys a universal scaling law, in the sense that the functional dependence of the flat-GSP spectrum is maintained up to a multiplication constant that depends solely on the particular geometric configuration of the system (i.e., the angle φ for a given ϵ_1 and ϵ_2). The results of our calculations were verified by performing rigorous electrodynamic simulations based on the FEM, to which a very good agreement was observed. We note, however, that the quasi-analytical model presented above not only provides more physical insight when gauged against numerical simulations, but is also far less computationally demanding and less time-consuming that the latter, since all the eigenmodes for a given structure can be determined at once from a single computation. Moreover, we have showed that WGPs and GPPs may be suitable candidates for versatile platforms (specially when taking advantage of the gate-tunability of graphene plasmons) to effectively route highly confined EM radiation. In this context, subsequent theoretical investigations of wedges/grooves with more realistic, rounded edges should constitute the basis of future work. The rounding of the apex leads to a slight decrease in the effective index of the plasmon modes, as shown by our finite-element simulations (cf. SI). Nevertheless, we expect our results to be qualitatively robust with respect to rounding. Furthermore, it was demonstrated that even for infinitely sharp metallic apexes, non-local effects prevent the emergence of singularities at the tip.[81] The case of a 2D layer deposited on a V-shaped substrate with a frequency-dependent dielectric function, e.g. a metal or a polar medium, can also be considered using the theory developed here. In addition, the effects of strain

owing to the folding of the 2D sheet around the apex remain largely unexplored in what concerns their implications in plasmonic excitations [for instance, in electronic transport it is well-known that strain introduces a scattering potential for the 2D Dirac fermions (via a gauge field) which can lead to the modification of the bandstructure].[82,83] We thus expect that this work will fuel future experimental realizations of WGPs/GGPs, as we believe that such modes may hold interesting implications for future all-photonic circuitries at the nanoscale.

Acknowledgement

PADG, SX and NAM acknowledge financial support from the Danish National Research Foundation through the sponsoring of the Center for Nanostructured Graphene (CNG), Project DNRF103. NMRP acknowledges funding from the European Commission within of the project "Graphene-Driven Revolutions in ICT and Beyond" (Ref. No. 696656), the Portuguese Foundation for Science and Technology (FCT) in the framework of the Strategic Financing UID/FIS/04650/2013, and the hospitality of the MackGraphe Center, Mackenzie Presbyterian University.

Supporting Information Available

Supporting Information Available: In the supporting information we describe the derivation of the equations given in the main article with utmost detail, while also outlining the calculation of the Green's function akin to a V-shaped interface between two insulators. Finally, we give further information about propagation losses, and critically analyze the dependence of the concurrently conducted finite element method (FEM) simulations on the radius of the curvature at the triangular apex, since the numerical simulations—contrarily to the analytics—cannot rigorously deal with the sharp tip of the V-structure.

This material is available free of charge via the Internet at `http://pubs.acs.org/`.

References

(1) Saleh, B. E. A.; Teich, M. C. *Fundamentals of Photonics*, 2nd ed.; Wiley, 2012.

(2) Atwater, H. A. The Promise of Plasmonics. *Sci. Am.* **2007**, *296*, 56–62.

(3) Maradudin, A. A.; Barnes, W. L.; Sambles, J. R. *Modern Plasmonics*; Elsevier, 2014.

(4) Maier, S. A. *Plasmonics: Fundamentals and Applications*; Springer: New York, 2007.

(5) Barnes, W. L.; Dereux, A.; Ebbesen, T. W. Surface plasmon subwavelength optics. *Nature* **2003**, *424*, 824–830.

(6) Armstrong, S. Plasmonics: Diffraction-free surface waves. *Nature Photon.* **2012**, *6*, 720.

(7) Barnes, W. L. Surface plasmon-polariton length scales: a route to sub-wavelength optics. *J. Opt. A: Pure Appl. Opt.* **2006**, *8*, S87.

(8) Gramotnev, D. K.; Bozhevolnyi, S. I. Plasmonics beyond the diffraction limit. *Nature Photon.* **2010**, *4*, 83–91.

(9) Ozbay, E. Plasmonics: Merging Photonics and Electronics at Nanoscale Dimensions. *Science* **2006**, *311*, 189–193.

(10) Bozhevolnyi, S. I.; Volkov, V. S.; Devaux, E.; Laluet, J.-Y.; Ebbesen, T. W. Channel plasmon subwavelength waveguide components including interferometers and ring resonators. *Nature* **2006**, *440*, 508–511.

(11) Han, Z.; Bozhevolnyi, S. I. Radiation guiding with surface plasmon polaritons. *Rep. Prog. Phys.* **2013**, *76*, 016402.

(12) Bozhevolnyi, S. I. *Plasmonic Nanoguides and Circuits*; Pan Stanford: Singapore, 2008.

(13) Bergman, D. J.; Stockman, M. I. Surface Plasmon Amplification by Stimulated Emission of Radiation: Quantum Generation of Coherent Surface Plasmons in Nanosystems. *Phys. Rev. Lett.* **2003**, *90*, 027402.

(14) Berini, P.; Leon, I. D. Surface plasmon-polariton amplifiers and lasers. *Nature Photon.* **2012**, *6*, 16–24.

(15) Ma, R.-M.; Oulton, R. F.; Sorger, V. J.; Zhang, X. Plasmon lasers: coherent light source at molecular scales. *Laser Photon. Rev.* **2013**, *7*, 1–21.

(16) Haffner, C. et al. All-plasmonic Mach-Zehnder modulator enabling optical high-speed communication at the microscale. *Nature Photon.* **2015**, *9*, 525.

(17) Chang, D. E.; Sørensen, A. S.; Hemmer, P. R.; Lukin, M. D. Quantum Optics with Surface Plasmons. *Phys. Rev. Lett.* **2006**, *97*, 053002.

(18) Heeres, R. W.; Kouwenhoven, L. P.; Zwiller, V. Quantum interference in plasmonic circuits. *Nature Nanotechnol.* **2013**, *8*, 719–722.

(19) Fakonas, J. S.; Lee, H.; Kelaita, Y. A.; Atwater, H. A. Two-plasmon quantum interference. *Nature Photon.* **2014**, *8*, 317–320.

(20) Tame, M. S.; McEnery, K. R.; Ozdemir, S. K.; Lee, J.; Maier, S. A.; Kim, M. S. Quantum plasmonics. *Nature Phys.* **2013**, *9*, 329–340.

(21) Bermudez-Urena, E.; Gonzalez-Ballestero, C.; Geiselmann, M.; Marty, R.; Radko, I. P.; Holmgaard, T.; Alaverdyan, Y.; Moreno, E.; García-Vidal, F. J.; Bozhevolnyi, S. I.; Quidant, R. Coupling of individual quantum emitters to channel plasmons. *Nature Commun.* **2015**, *6*, 7883.

(22) Aćimović, S. S.; Ortega, M. A.; Sanz, V.; Berthelot, J.; Garcia-Cordero, J. L.; Renger, J.; Maerkl, S. J.; Kreuzer, M. P.; Quidant, R. LSPR Chip for Parallel, Rapid, and Sensitive Detection of Cancer Markers in Serum. *Nano Lett.* **2014**, *14*, 2636–2641.

(23) Haes, A. J.; Haynes, C. L.; McFarland, A. D.; Schatz, G. C.; Duyne, R. P. V.; Zou, S. Plasmonic Materials for Surface-Enhanced Sensing and Spectroscopy. *MRS Bulletin* **2005**, *30*, 368–375.

(24) Brolo, A. G. Plasmonics for future biosensors. *Nature Photon.* **2012**, *6*, 709–713.

(25) Long, Y.-T.; Jing, C. *Localized Surface Plasmon Resonance Based Nanobiosensors*; Springer, 2014.

(26) Rodrigo, D.; Limaj, O.; DavideJanner,; Etezadi, D.; García de Abajo, F. J.; Pruneri, V.; Altug, H. Mid-infrared plasmonic biosensing with graphene. *Science* **2015**, *349*, 165–168.

(27) Fang, N.; Lee, H.; Sun, C.; Zhang, X. Sub-Diffraction-Limited Optical Imaging with a Silver Superlens. *Science* **2005**, *308*, 534–537.

(28) Liu, N.; Hentschel, M.; Weiss, T.; Alivisatos, A. P.; Giessen, H. Three-Dimensional Plasmon Rulers. *Science* **2011**, *332*, 1407–1410.

(29) Vo-Dinh, T.; Fales, A. M.; Griffin, G. D.; Khoury, C. G.; Liu, Y.; Ngo, H.; Norton, S. J.; Register, J. K.; Wang, H.-N.; Yuan, H. Plasmonic nanoprobes: from chemical sensing to medical diagnostics and therapy. *Nanoscale* **2013**, *5*, 10127–10140.

(30) Zheng, Y. B.; Kiraly, B.; Weiss, P. S.; Huang, T. J. Molecular plasmonics for biology and nanomedicine. *Nanomedicine* **2012**, *7*, 751 – 770.

(31) Bardhan, R.; Lal, S.; Joshi, A.; Halas, N. J. Theranostic Nanoshells: From Probe Design to Imaging and Treatment of Cancer. *Accounts of Chemical Research* **2011**, *44*, 936–946.

(32) Fang, Y.; Sun, M. Nanoplasmonic waveguides: towards applications in integrated nanophotonic circuits. *Light Sci. Appl.* **2015**, *4*, e294.

(33) Krenn, J. R. Nanoparticle waveguides: Watching energy transfer. *Nature Mater.* **2003**, *2*, 210–211.

(34) Maier, S. A.; Kik, P. G.; Atwater, H. A.; Meltzer, S.; Harel, E.; Koel, B. E.; Requicha, A. A. G. Local detection of electromagnetic energy transport below the diffraction limit in metal nanoparticle plasmon waveguides. *Nature Mater.* **2003**, *2*, 229–232.

(35) Alù, A.; Belov, P. A.; Engheta, N. Coupling and guided propagation along parallel chains of plasmonic nanoparticles. *New J. Phys.* **2011**, *13*, 033026.

(36) Smith, C. L. C.; Stenger, N.; Kristensen, A.; Mortensen, N. A.; Bozhevolnyi, S. I. Gap and channeled plasmons in tapered grooves: a review. *Nanoscale* **2015**, *7*, 9355–9386.

(37) Gramotnev, D. K.; Bozhevolnyi, S. I. Nanofocusing of electromagnetic radiation. *Nature Photon.* **2014**, *9*, 13–22.

(38) Raza, S.; Stenger, N.; Pors, A.; Holmgaard, T.; Kadkhodazadeh, S.; Wagner, J. B.; Pedersen, K.; Wubs, M.; Bozhevolnyi, S. I.; Mortensen, N. A. Extremely confined gap surface-plasmon modes excited by electrons. *Nature Commun.* **2014**, *5*, 4125.

(39) Pile, D. F. P.; Gramotnev, D. K. Channel plasmon–polariton in a triangular groove on a metal surface. *Opt. Lett.* **2004**, *29*, 1069–1071.

(40) Moreno, E.; García-Vidal, F. J.; Rodrigo, S. G.; Martin-Moreno, L.; Bozhevolnyi, S. I. Channel plasmon-polaritons: modal shape, dispersion, and losses. *Opt. Lett.* **2006**, *31*, 3447–3449.

(41) Li, X.; Jiang, T.; Shen, L.; Deng, X. Subwavelength guiding of channel plasmon polaritons by textured metallic grooves at telecom wavelengths. *Appl. Phys. Lett.* **2013**, *102*, 031606.

(42) Volkov, V. S.; Bozhevolnyi, S. I.; Devaux, E.; Ebbesen, T. W. Compact gradual bends for channel plasmon polaritons. *Opt. Express* **2006**, *14*, 4494–4503.

(43) Dobrzynski, L.; Maradudin, A. A. Electrostatic Edge Modes in a Dielectric Wedge. *Phys. Rev. B* **1972**, *6*, 3810–3815.

(44) Boardman, A. D.; Aers, G. C.; Teshima, R. Retarded edge modes of a parabolic wedge. *Phys. Rev. B* **1981**, *24*, 5703–5712.

(45) Boardman, A. D.; Garcia-Molina, R.; Gras-Marti, A.; Louis, E. Electrostatic edge modes of a hyperbolic dielectric wedge: Analytical solution. *Phys. Rev. B* **1985**, *32*, 6045–6047.

(46) Novikov, I. V.; Maradudin, A. A. Channel polaritons. *Phys. Rev. B* **2002**, *66*, 035403.

(47) Lu, J. Q.; Maradudin, A. A. Channel plasmons. *Phys. Rev. B* **1990**, *42*, 11159–11165.

(48) Volkov, V. S.; Bozhevolnyi, S. I.; Rodrigo, S. G.; Martín-Moreno, L.; García-Vidal, F. J.; Devaux, E.; Ebbesen, T. W. Nanofocusing with Channel Plasmon Polaritons. *Nano Lett.* **2009**, *9*, 1278–1282.

(49) Bozhevolnyi, S. I.; Nerkararyan, K. V. Channel plasmon polaritons guided by graded gaps: closed-form solutions. *Opt. Express* **2009**, *17*, 10327–10334.

(50) Bozhevolnyi, S. I.; Nerkararyan, K. V. Analytic description of channel plasmon polaritons. *Opt. Lett.* **2009**, *34*, 2039–2041.

(51) Luo, Y.; Pendry, J. B.; Aubry, A. Surface Plasmons and Singularities. *Nano Letters* **2010**, *10*, 4186–4191.

(52) Geim, A. K. Graphene: Status and Prospects. *Science* **2009**, *324*, 1530–1534.

(53) Castro Neto, A. H.; Guinea, F.; Peres, N. M. R.; Novoselov, K. S.; Geim, A. K. The electronic properties of graphene. *Rev. Mod. Phys.* **2009**, *81*.

(54) Gonçalves, P. A. D.; Peres, N. M. R. *An Introduction to Graphene Plasmonics*; World Scientific: Singapore, 2016.

(55) García de Abajo, F. J. Graphene Plasmonics: Challenges and Opportunities. *ACS Photonics* **2014**, *1*, 135–152.

(56) Xiao, S.; Zhu, X.; Li, B.-H.; Mortensen, N. A. Graphene-plasmon polaritons: From fundamental properties to potential applications. *Front. Phys.* **2016**, *11*, 117801.

(57) Bludov, Y. V.; Ferreira, A.; Peres, N. M. R.; Vasilevskiy, M. I. A Primer on Surface Plasmon-Polaritons in Graphene. *Int. J. Mod. Phys. B* **2013**, *27*, 1341001.

(58) Low, T.; Avouris, P. Graphene Plasmonics for Terahertz to Mid-Infrared Applications. *ACS Nano* **2014**, *8*, 1086–1101.

(59) Koppens, F. H. L.; Chang, D. E.; García de Abajo, F. J. Graphene Plasmonics: A Platform for Strong Light-Matter Interactions. *Nano Lett.* **2011**, *11*, 3370–3377.

(60) Ju, L.; Geng, B.; Horng, J.; Girit, C.; Martin, M.; Hao, Z.; Bechtel, H. A.; Liang, X.; Zettl, A.; Shen, Y. R.; Wang, F. Graphene plasmonics for tunable terahertz metamaterials. *Nature Nanotechnol.* **2011**, *6*, 630–634.

(61) Yan, H.; Low, T.; Zhu, W.; Wu, Y.; Freitag, M.; Li, X.; Guinea, F.; Avouris, P.; Xia, F. Damping pathways of mid-infrared plasmons in graphene nanostructures. *Nature Photon.* **2013**, *7*, 394–399.

(62) Luxmoore, I. J.; Gan, C. H.; Liu, P. Q.; Valmorra, F.; Li, P.; Faist, J.; Nash, G. R. Strong coupling in the far-infrared between graphene plasmons and the surface optical phonons of silicon dioxide. *ACS Photonics* **2014**, *1*, 1151.

(63) Hu, H.; Yang, X.; Zhai, F.; Hu, D.; Liu, R.; Liu, K.; Sun, Z.; Dai, Q. Far-field nanoscale infrared spectroscopy of vibrational fingerprints of molecules with graphene plasmons. *Nature Commun.* **2016**, *7*, 1151.

(64) Yan, H.; Xia, F.; Li, Z.; Avouris, P. Plasmonics of coupled graphene micro-structures. *New J. Phys.* **2012**, *14*, 125001.

(65) Fang, Z.; Thongrattanasiri, S.; Schlather, A.; Liu, Z.; Ma, L.; Wang, Y.; Ajayan, P. M.;

Nordlander, P.; Halas, N. J.; García de Abajo, F. J. Gated Tunability and Hybridization of Localized Plasmons in Nanostructured Graphene. *ACS Nano* **2013**, *7*, 2388–2395.

(66) Fang, Z.; Wang, Y.; Schlather, A. E.; Liu, Z.; Ajayan, P. M.; García de Abajo, F. J.; Nordlander, P.; Zhu, X.; Halas, N. J. Active Tunable Absorption Enhancement with Graphene Nanodisk Arrays. *Nano Lett.* **2014**, *14*, 299–304.

(67) Zhu, X.; Wang, W.; Yan, W.; Larsen, M. B.; Bøggild, P.; Pedersen, T. G.; Xiao, S.; Zi, J.; Mortensen, N. A. Plasmon-Phonon Coupling in Large-Area Graphene Dot and Antidot Arrays Fabricated by Nanosphere Lithography. *Nano Lett.* **2014**, *14*, 2907–2913.

(68) Wang, Z.; Li, T.; Almdal, K.; Mortensen, N. A.; Xiao, S.; Ndoni, S. Pushing graphene plasmon polaritons to the near-infrared window by block copolymer nanolithography. *arXiv:1606.02471 [physics.optics]* **2016**,

(69) Liu, P. Q.; Valmorra, F.; Maissen, C.; Faist, J. Electrically tunable graphene anti-dot array terahertz plasmonic crystals exhibiting multi-band resonances. *Optica* **2015**, *2*, 135–140.

(70) Yeung, K. Y. M.; Chee, J.; Yoon, H.; Song, Y.; Kong, J.; Ham, D. Far-Infrared Graphene Plasmonic Crystals for Plasmonic Band Engineering. *Nano Lett.* **2014**, *14*, 2479–2484.

(71) Liu, P.; Zhang, X.; Ma, Z.; Cai, W.; Wang, L.; Xu, J. Surface plasmon modes in graphene wedge and groove waveguides. *Opt. Express* **2013**, *21*, 32432–32440.

(72) Kim, K.; Lee, Z.; Malone, B. D.; Chan, K. T.; Alemán, B.; Regan, W.; Gannett, W.; Crommie, M. F.; Cohen, M. L.; Zettl, A. Multiply folded graphene. *Phys. Rev. B* **2011**, *83*, 245433.

(73) Pakhnevich, A. A.; Golod, S. V.; Prinz, V. Y. Surface melting of copper during graphene growth by chemical vapour deposition. *J. Phys. D: Appl. Phys.* **2015**, *48*, 435303.

(74) Song, Q.; An, M.; Chen, X.; Peng, Z.; Zang, J.; Yang, N. Adjustable thermal resistor by reversibly folding a graphene sheet. *Nanoscale* **2016**,

(75) Zhu, W.; Low, T.; Perebeinos, V.; Bol, A. A.; Zhu, Y.; Yan, H.; Tersoff, J.; Avouris, P. Structure and Electronic Transport in Graphene Wrinkles. *Nano Lett.* **2012**, *12*, 3431–3436.

(76) Wu, J.-W.; Hawrylak, P.; Eliasson, G.; Quinn, J.; Fetter, A. Magnetoplasma surface waves on the lateral surface of a semiconductor superlattice. *Sol. State Commun.* **1986**, *58*, 795–798.

(77) Wang, W.; Apell, P.; Kinaret, J. Edge plasmons in graphene nanostructures. *Phys. Rev. B* **2011**, *84*, 085423.

(78) Abramowitz, M.; Stegun, I. A. *Handbook of Mathematical Functions: with Formulas, Graphs, and Mathematical Tables*; Dover: New York, 1965.

(79) Harrison, P. *Quantum Wells, Wires and Dots*, 3rd ed.; Wiley, 2010.

(80) Nielsen, R. B.; Fernandez-Cuesta, I.; Boltasseva, A.; Volkov, V. S.; Bozhevolnyi, S. I.; Klukowska, A.; Kristensen, A. Channel plasmon polariton propagation in nanoimprinted V-groove waveguides. *Opt. Lett.* **2008**, *33*, 2800–2802.

(81) Toscano, G.; Raza, S.; Yan, W.; Jeppesen, C.; Xiao, S.; Wubs, M.; Jauho, A.-P.; Bozhevolnyi, S. I.; Mortensen, N. A. Nonlocal response in plasmonic waveguiding with extreme light confinement. *Nanophotonics* **2013**, *2*, 161–166.

(82) de Juan, F.; Mañes, J. L.; Vozmediano, M. A. H. Gauge fields from strain in graphene. *Phys. Rev. B* **2013**, *87*, 165131.

(83) Amorim, B.; Cortijo, A.; de Juan, F.; Grushin, A.; Guinea, F.; Gutiérrez-Rubio, A.; Ochoa, H.; Parente, V.; Roldán, R.; San-Jose, P.; Schiefele, J.; Sturla, M.; Vozmediano, M. Novel effects of strains in graphene and other two dimensional materials.

Physics Reports **2016**, *617*, 1 – 54, Novel effects of strains in graphene and other two dimensional materials.

Graphical TOC Entry

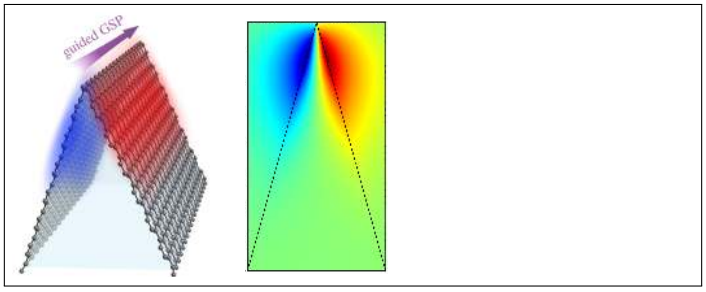

Supporting Information for: Graphene Plasmons in Triangular Wedges and Grooves

P. A. D. Gonçalves,[*,†,‡] E. J. C. Dias,[¶] Sanshui Xiao,[†,‡] M. I. Vasilevskiy,[¶] N. Asger Mortensen,[†,‡] and N. M. R. Peres[*,¶]

†*Department of Photonics Engineering, Technical University of Denmark, DK-2800 Kgs. Lyngby, Denmark*

‡*Center for Nanostructured Graphene, Technical University of Denmark, DK-2800 Kgs. Lyngby, Denmark*

¶*Department of Physics and Center of Physics, University of Minho, PT-4710–057, Braga, Portugal*

E-mail: padgo@fotonik.dtu.dk; peres@fisica.uminho.pt

Abstract

We derive, in the electrostatic limit, the dispersion relation for graphene plasmons (GPs) supported by a triangular-like interface between two dielectric media. These graphene channel plasmons possess as main characteristics the ability to confine the electric field also in the lateral direction and act as subwavelength one-dimensional (1D) waveguides. In this supporting information we describe the derivation of the equations given in the main article with utmost detail, while also outlining the calculation of the Green's function akin to a V-shaped interface between two insulators. Propagation losses are also discussed, and compared against the losses of flat-GPs. Finally, we

critically analyze the dependence of the concurrently conducted finite element method (FEM) simulations on the radius of the curvature at the triangular apex, since the numerical simulations—contrarily to the analytics—cannot rigorously cope with the infinitely sharp edge of the V-structure.

Statement of the problem

For the sake of clarity we consider only wedge graphene plasmon (WGP) modes. The derivation for the groove follows by exploiting the symmetries with respect to the interchange of dielectric constants or the replacement $\varphi \to \pi - \varphi$.

In order to derive the plasmon modes supported by a dielectric wedge covered with graphene in the electrostatic limit, we need to solve Poisson's equation,

$$\nabla^2 \Phi(\mathbf{r}) = -\frac{\rho(\mathbf{r})}{\epsilon_0} \ . \tag{S1}$$

The one-dimensional (1D) wedge possesses translational symmetry along the z-direction; therefore, we decompose both the electrostatic potential and the charge-density as (in cylindrical coordinates)

$$\Phi(\mathbf{r}) = \Phi(r,\theta)e^{iqz} \ , \tag{S2}$$

$$\rho(\mathbf{r}) = \rho(r,\theta)e^{iqz} \ , \tag{S3}$$

where we have omitted the usual time-dependence of the form $e^{-i\omega t}$ for the sake of clarity. The above procedure effectively transforms a three-dimensional (3D) problem into a two-dimensional (2D) one:

$$\nabla_{2D}^2 \Phi(r,\theta) - q^2 \Phi(r,\theta) = -\frac{\rho(r,\theta)}{\epsilon_0} \ , \tag{S4}$$

where $\nabla_{2D}^2 = \partial_r^2 + r^{-1}\partial_r + r^{-2}\partial_\theta^2$ is the transverse part of the Laplacian in cylindrical coordinates.

The solution of Eq. (S4) yields the wedge graphene plasmons (WGPs) that propagate along the longitudinal direction. To find such modes, first we need to compute the Green's function for a wedge-like interface between two dielectric media.[1,2] That exercise is the subject of the next section.

Green's function of a wedge-like interface

The Green's functions of a wedge-like interface between two materials with relative permittivities ϵ_1 and ϵ_2, as shown in Fig. S1, are defined through the expressions,

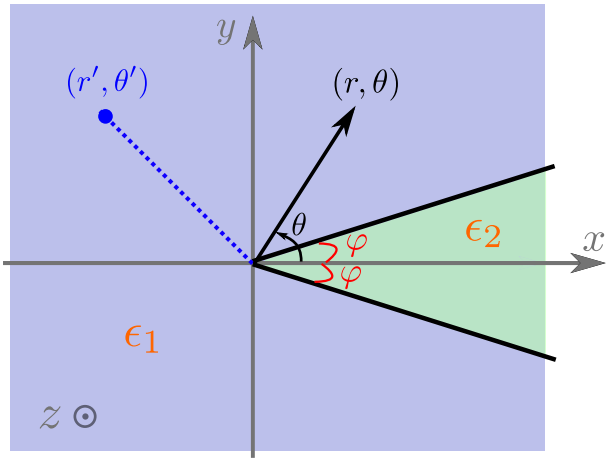

Figure S1: Wedge interface—with an opening angle of 2φ—between two dielectric media characterized by relative permittivities ϵ_2 (for $-\varphi \leq \theta \leq \varphi$) and ϵ_1 (for $\varphi \leq \theta \leq 2\pi - \varphi$).

$$\left[\frac{\partial^2}{\partial r^2} + \frac{1}{r}\frac{\partial}{\partial r} + \frac{1}{\partial r^2}\frac{\partial^2}{\partial \theta^2} - q^2\right] G_1(r,\theta;r',\theta') = -\frac{\delta(r-r')\delta(\theta-\theta')}{\epsilon_1\epsilon_0 r} \ , \tag{S5}$$

for for $\varphi \leq \theta \leq 2\pi - \varphi$, and

$$\left[\frac{\partial^2}{\partial r^2} + \frac{1}{r}\frac{\partial}{\partial r} + \frac{1}{\partial r^2}\frac{\partial^2}{\partial \theta^2} - q^2\right] G_2(r,\theta;r',\theta') = 0 \ , \tag{S6}$$

for $-\varphi \leq \theta \leq \varphi$. The boundary conditions connect the Green's function in both regions of the structure (these will be introduced explicitly shortly). We will determine the solution of

Eqs. (S5) and (S6) by using the solutions of the corresponding homogeneous problem (which is a particular solution of the inhomogeneous problem) as a basis to construct the (general) solution of the above equations (subjected to the proper boundary conditions).[1,2]

To make the problem more amenable to handle we shall treat the cases of even and odd symmetries separately. Therefore, we will only need to solve the problem in, say, the upper-half space (i.e., $y \geq 0$ or $0 \leq \theta \leq \pi$).

Even symmetry case

The solution of the homogeneous equation corresponding to Eqs. (S5) and (S6) is separable in a radial part, whose eigenfunctions are modified Bessel functions of imaginary order $K_{i\mu}(x)$, and an angular part, whose eigenfunctions are hyperbolic trigonometric functions. The variable μ must satisfy $\Re\mathrm{e}\{\mu\} \geq 0$ since we are looking for plasmonic modes. Thus, for the even case, the Green's function characterizing the potential felt at (r, θ), in the absence of graphene, due to an elementary charge placed at (r', θ') then reads

$$G_2^e(r,\theta;r',\theta') = \int_0^\infty d\mu K_{i\mu}(qr) A_\mu^e \cosh(\mu\theta) \quad ; \quad 0 \leq \theta \leq \varphi \ , \tag{S7}$$

$$G_+^e(r,\theta;r',\theta') = \int_0^\infty d\mu K_{i\mu}(qr) \left[B_\mu^e \cosh(\mu\theta) + C_\mu^e \sinh(\mu\theta)\right] \quad ; \quad \varphi \leq \theta \leq \theta' \ , \tag{S8}$$

$$G_-^e(r,\theta;r',\theta') = \int_0^\infty d\mu K_{i\mu}(qr) D_\mu^e \cosh[\mu(\pi-\theta)] \quad ; \quad \theta' \leq \theta \leq \pi \ , \tag{S9}$$

where the coefficients A_μ^e to D_μ^e are determined by imposing the boundary conditions holding for this system, namely

$$G_2^e(r,\theta;r',\theta')|_{\theta=\varphi} = G_+^e(r,\theta;r',\theta')|_{\theta=\varphi} \ , \tag{S10}$$

$$\epsilon_2 \frac{\partial}{\partial\theta} G_2^e(r,\theta;r',\theta')|_{\theta=\varphi} = \epsilon_1 \frac{\partial}{\partial\theta} G_+^e(r,\theta;r',\theta')|_{\theta=\varphi} \ , \tag{S11}$$

$$G_+^e(r,\theta;r',\theta')|_{\theta=\theta'} = G_-^e(r,\theta;r',\theta')|_{\theta=\theta'} \ , \tag{S12}$$

$$\frac{\partial}{\partial\theta} G_-^e(r,\theta;r,\theta')|_{\theta=\theta'} - \frac{\partial}{\partial\theta} G_+^e(r,\theta;r',\theta')|_{\theta=\theta'} = -\frac{r}{\epsilon_1\epsilon_0}\delta(r-r') \ . \tag{S13}$$

Equations (S10)-(S13) form a linear system for the coefficients A^e_μ to D^e_μ. After some algebra, one finds that

$$A^e_\mu = \frac{2T}{\pi^2\epsilon_2\epsilon_0} K_{i\mu}(qr') \frac{\sinh(\mu\pi)\cosh[\mu(\pi-2\theta')]}{\sinh(\mu\pi) - R\sinh[\mu(\pi-2\varphi)]} \ , \tag{S14}$$

[where the result $\int_0^\infty \frac{dx}{x} K_{i\mu}(x)K_{i\mu'}(x) = \frac{\pi^2\delta(\mu-\mu')}{2\mu\sinh(\pi\mu)}$ (for $\mu,\mu'>0$) has been used[3]] with

$$R = \frac{\epsilon_2 - \epsilon_1}{\epsilon_2 + \epsilon_1} \ , \tag{S15}$$

$$T = \frac{2\epsilon_2}{\epsilon_2 + \epsilon_1} \ , \tag{S16}$$

along with similar expressions for the remaining coefficients (not shown for brevity). However, we will only need the A_μ in what follows, since we will be evaluating it at the interface (where the charges are, that is, within the graphene monolayer).

Odd symmetry case

Following the same guidelines that lead to Eq. (S14), with the appropriate adaptations, one obtains

$$A^o_\mu = \frac{2T}{\pi^2\epsilon_2\epsilon_0} K_{i\mu}(qr') \frac{\sinh(\mu\pi)\sinh[\mu(\pi-2\theta')]}{\sinh(\mu\pi) + R\sinh[\mu(\pi-2\varphi)]} \ , \tag{S17}$$

corresponding to the odd-symmetry Green's function in medium 2, that is,

$$G^o_2(r,\theta;r',\theta') = \int_0^\infty d\mu K_{i\mu}(qr) A^o_\mu \sinh(\mu\theta) \quad ; \quad 0 \le \theta \le \varphi \ . \tag{S18}$$

Summary: Green's functions (even and odd)

In possession of Eqs. (S7), (S14) and (S17)-(S18), we may write

$$G^e_2(r,\theta;r',\theta') = \frac{2T}{\pi^2\epsilon_2\epsilon_0} \int_0^\infty d\mu K_{i\mu}(qr) K_{i\mu}(qr') \Omega^e(\theta,\theta') \ , \tag{S19}$$

where we have introduced the function,

$$\Omega^e(\theta,\theta') = \frac{\sinh(\mu\pi)\cosh(\mu\theta)\cosh[\mu(\pi-2\theta')]}{\sinh(\mu\pi) - R\sinh[\mu(\pi-2\varphi)]} \ , \tag{S20}$$

and,

$$G_2^o(r,\theta;r',\theta') = \frac{2T}{\pi^2\epsilon_2\epsilon_0}\int_0^\infty d\mu K_{i\mu}(qr)K_{i\mu}(qr')\Omega^o(\theta,\theta') \ , \tag{S21}$$

with

$$\Omega^o(\theta,\theta') = \frac{\sinh(\mu\pi)\sinh(\mu\theta)\sinh[\mu(\pi-2\theta')]}{\sinh(\mu\pi) + R\sinh[\mu(\pi-2\varphi)]} \ . \tag{S22}$$

Note that, naturally, the only difference between the even and odd symmetry Green's functions is encapsulated in the functions $\Omega^{e/o}(\theta,\theta')$ which contain all the angular dependence.

The Green's functions in medium 1 may be derived following similar steps.

Remark: for the particular case where $\varphi = \pi/2$, the above Green's functions are not a suitable representations for those of a planar interface. This is because the homogeneous solutions of the corresponding Laplace equation are no longer the same as in the cylindrical symmetry case, and therefore our procedure above would need to be adapted accordingly for that specific case—see, for instance, Ref. 4 for further details.

Graphene Plasmons in the Wedge Geometry

Having derived the Green's functions of a wedge-like interface, we can now proceed towards the solution of Poisson's equation [cf. Eq. (S4)],

$$\left[\frac{\partial^2}{\partial r^2} + \frac{1}{r}\frac{\partial}{\partial r} + \frac{1}{\partial r^2}\frac{\partial^2}{\partial\theta^2} - q^2\right]\Phi(r,\theta) = -\frac{\rho(r,\theta)}{\epsilon_0} \ , \tag{S23}$$

whose solution may, in general, be written as

$$\Phi(r,\theta) = \int_0^\infty dr' r' \int_0^{2\pi} d\theta' G_2(r,\theta;r',\theta')\rho(r',\theta') \ . \tag{S24}$$

Here, the density of charge carriers may be expressed in the form

$$\rho(r,\theta) = -e\ n(r)\frac{\delta(\theta-\varphi)}{r} \ , \tag{S25}$$

where $n(r)$ accounts for the 2D particle-density along the radial coordinate. On the other hand, the 2D continuity equation dictates (in frequency domain)

$$\begin{aligned} n(r) &= \frac{i}{\omega e}\nabla_{2D}\cdot\mathbf{J}_{2D} \\ &= \frac{\sigma(\omega)}{i\omega e}\left[\frac{\partial^2}{\partial r^2} - q^2\right]\Phi(r,\varphi) \ , \end{aligned} \tag{S26}$$

where, in the last equality, we have employed Ohm's law, and where $\sigma(\omega)$ denotes the dynamical conductivity of graphene. Having an explicit expression for $n(r)$, one may now use Eqs. (S25) and (S26) to simplify Eq. (S24) substantially, in particular

$$\Phi(r,\theta) = \frac{i\sigma(\omega)}{\omega}\int_0^\infty dr' G_2(r,\theta;r',\varphi)\left[\frac{\partial^2}{\partial r'^2} - q^2\right]\Phi(r',\varphi) \ . \tag{S27}$$

Notice that the potential in the *whole space* can only be derived once the potential *at the graphene sheet* is determined. The determination of $\Phi(r',\varphi)$ is outlined below.

Solution of $\Phi(r',\varphi)$ via orthogonal polynomials expansion

Equation (S27), at $\theta = \varphi$, reduces to

$$\phi(r) = \frac{i\sigma(\omega)}{\omega}\int_0^\infty dr' G_2(r,\varphi;r',\varphi)\left[\frac{\partial^2}{\partial r'^2} - q^2\right]\phi(r') \ . \tag{S28}$$

Here, we have defined $\phi(r) \equiv \Phi(r', \varphi)$. The previous equation stands as an integro-differential equation for the scalar potential $\phi(r)$, and we are not aware of an analytical solution. In what follows, we will solve Eq. (S28) using the orthogonal polynomials expansion technique;[5–7] within this approach, it is possible to convert the above integro-differential equation into a standard linear algebra eigenproblem. To that end, we expand the electric potential at $\theta = \varphi$ using Laguerre polynomials, $L_n(x)$ as a complete set of basis functions, namely

$$\phi(r) = \sum_{n=0}^{\infty} c_n L_n(qr) e^{-qr/2} \ . \tag{S29}$$

In order to arrive at an eigenvalue problem, all we need to do is to substitute this expansion into both sides of Eq. (S28), followed by the exploitation of the orthogonality of Laguerre polynomials $\left[\text{explicitly, } \int_0^\infty dx\ e^{-x} L_n(x) L_m(x) = \delta_{n,m}\right]$.[8] Such procedure leads to the following matrix equation

$$\frac{i\omega}{q\sigma(\omega)} c_m = \sum_{n=0}^{N} U_{mn} c_n \ , \tag{S30}$$

where we have truncated the expansion in Eq. (S29) at N, and the elements of the matrix $\mathbf{U}$ [of size $(N+1) \times (N+1)$] read

$$U_{mn} = -\int_0^\infty dy \int_0^\infty dx G_2(x, \varphi; y, \varphi) e^{-\frac{x+y}{2}} L_m(x) \left[L_{n-2}^{(2)}(y) + L_{n-1}^{(1)}(y) - \frac{3}{4} L_n(y) \right] \ , \tag{S31}$$

where the dimensionless variables $x = qr$ and $y = qr'$ have been introduced, and $L_n^{(k)}(x)$ refer to the generalized Laguerre polynomials.[8] We note that both the integration over x and y can be performed analytically; then, only the integration over μ [which enters via the Green's function—cf. Eqs. (S19) and (S21)] needs to be carried out numerically. This makes the computation of the matrix elements extremely fast. The eigenvalue equation (S30) can be solved numerically using standard linear algebra routines. Once we find the corresponding eigenvalues (whose number matches the size of the vector $\vec{c}$, that is, $N+1$), the spectrum

of graphene plasmons traveling along the triangular wedge follows from

$$\frac{i\omega}{q\sigma(\omega)} = \tilde{\lambda}_n \ , \tag{S32}$$

where, for a given frequency, Eq. (S32) returns the discrete wedge GPs modes. In particular, using graphene's Drude-like conductivity with negligible damping,[7] one obtains the following relation for the dispersion relation of wedge graphene plasmons (WGPs) [and for grooves alike],

$$\Omega(q) = \Omega_{\text{flat}}(q)\frac{2}{\pi}\sqrt{\lambda_n} \ , \tag{S33}$$

where the (re)defined eigenvalues λ_n stem from $\tilde{\lambda}_n = \frac{2T}{\pi^2\epsilon_2\epsilon_0}\lambda_n = \frac{4\lambda_n}{\pi^2\epsilon_0(\epsilon_1+\epsilon_2)}$, that is, we have explicitly factorized the proportionality factor $\frac{2T}{\pi^2\epsilon_2\epsilon_0}$ appearing in the Green's function (S21). The above equation gives the WGP's energy, $\Omega(q)$, parameterized by the propagation constant along the apex of the wedge. Here, $\Omega_{\text{flat}}(q) = \sqrt{\frac{4\alpha}{\epsilon_1+\epsilon_2}E_F\hbar c q}$ stands for the dispersion relation for plasmons in flat graphene (sandwiched between two dielectrics with ϵ_1 and ϵ_2; α denotes the fine-structure constant). Note that the spectrum of WGPs contains a discrete set of even and odd modes [depending of whether we use $G_2^e(x,\varphi;y,\varphi)$ or $G_2^o(x,\varphi;y,\varphi)$ in Eq. (S31)].

The dispersion relation akin to the first three waveguide-like wedge graphene plasmons is shown in Fig. S2, obtained by virtue of Eq. (S33). It is interesting to note that, within our theory, the spectrum of each WGPs mode is simply the spectrum of a flat GPs multiplied by a proportionality constant related to the corresponding eigenvalue, as Eq. (S33) and Fig. S2 plainly show. This proportionality constant, as highlighted in the main manuscript, depends uniquely in the opening angles, 2φ, and material parameters, and therefore carries a purely geometric meaning.

By solving the linear algebra problem posed by Eq. (S30) we can now reconstruct any

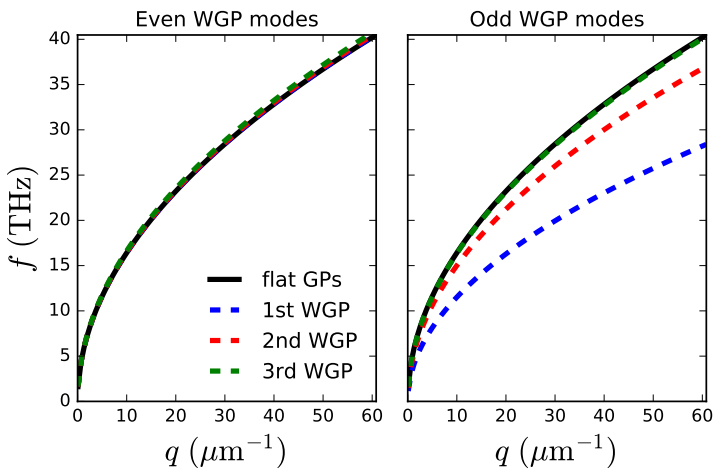

Figure S2: Dispersion relation of graphene plasmons—with even and odd symmetry—guided along a graphene-covered dielectric wedge (first three modes), obtained using Eq. (S33). The solid black line depicts the spectrum of plasmons in a flat graphene. Parameters: $E_F = 0.4$ eV, $\epsilon_1 = 1$, $\epsilon_2 = 4$, and $2\varphi = 25°$. We have used $N = 12$ for the truncation of the sum/matrix.

physical quantity we want from the corresponding calculated eigenvalues and eigenvectors. Recall that the (radial) electrostatic potential evaluated at $\theta = \varphi$ (the graphene sheet), according to Eq. (S29), has the form

$$\Phi(r,\varphi) = \phi(r) = \sum_n c_n L_n(qr) e^{-qr/2} \ . \tag{S34}$$

The transverse part of the electric field then follows from

$$\mathbf{E}(r,\theta) = -\nabla_{2D}\Phi(r,\theta) \ , \tag{S35}$$

Alternatively, in cartesian coordinates, the components of the electric field in the xy-plane read

$$\begin{pmatrix} E_x \\ E_y \end{pmatrix} = \begin{pmatrix} \cos\varphi & -\sin\varphi \\ \sin\varphi & \cos\varphi \end{pmatrix} \begin{pmatrix} E_r \\ E_\theta \end{pmatrix} \ . \tag{S36}$$

We further note that—for small opening angles— the θ-component of the electric field is approximately equal to the component of the electric field projected along the y-axis, that

is, $E_\theta(x,y) \simeq E_y(x,y)$.

Propagation losses

Loss is a well-known issue in plasmonics. Here, we shall briefly comment and compare the propagation losses of the WGP/GPP modes against their flat-GP counterpart. To that end, we cast Eq. (S32) as

$$q = f\frac{1}{\tilde{\lambda}_n} \quad \Rightarrow \quad q \propto \frac{1}{\tilde{\lambda}_n} \propto \frac{1}{\lambda_n} \ , \tag{S37}$$

where the proportionality factor is $f = i\omega/\sigma(\omega)$. Losses can be quantified by introducing the *propagation length*, L_p, which is defined as $L_p = (2\Im\mathrm{m}\ q)^{-1}$, and essentially corresponds to the distance the plasmon propagates until its intensity falls off by $1/e$. Hence, its value decreases with increasing loss. Therefore, in the light of Eq. (S37) one can write

$$L_p = \frac{\tilde{\lambda}_n}{2\Im\mathrm{m}\ f} \propto \lambda_n \ . \tag{S38}$$

Since λ_n increases with the mode order (up to $\pi^2/4$, corresponding to flat graphene), then the propagation length is diminishes from the higher-order modes to the fundamental one. This is shown in figure's S3 a) panel. Note, however, that the corresponding field confinement is largest for the fundamental mode. This trade-off between field confinement and loss is characteristic of plasmonics. Still, multi-micrometer propagation can be easily obtained at THz frequencies.

A perhaps more interesting result emerges when we compare the propagation length with the corresponding plasmon wavelength. Such procedure indicates the number of plasmon oscillations that occur within the propagation length. This is a much more fair comparison because it measures the *ratio* between field localization and losses. The outcome is presented in figure's S3 b) panel. There are two major features: first there is a maximum value for $L_p/\lambda_{\mathrm{WGP}}$ (do not confuse it with the eigenvalue λ_n); second, and more importantly, one can

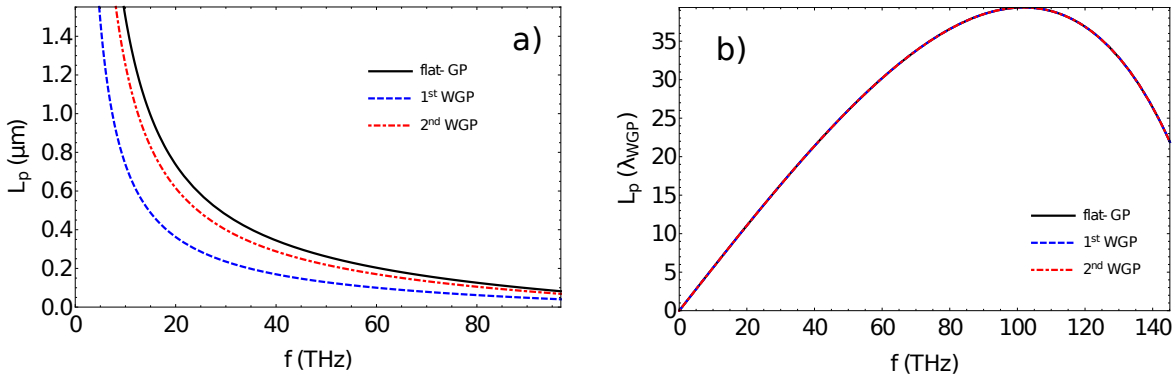

Figure S3: Propagation loss. Left: propagation length in absolute units for the flat-GP (black line) and the two lowest-energy WGP modes for a graphene-covered wedge with an opening angle of $2\varphi = 25°$, $E_F = 0.4$ eV, $\hbar\gamma = 3.7$ meV[9], $\epsilon_1 = 1$ and $\epsilon_2 = 4$ (similar results can be obtained for grooves). Rigth: propagation length in units of the graphene plasmon wavelength corresponding to each mode. Graphene conductivity was modeled according to Kubo's formula (both intra- and inter-band contributions) at zero temperature.[7]

observe that the ratio $L_p/\lambda_{\rm WGP}$, at any frequency, remains the same despite the mode order, and it is fact the same as for the flat-GP. Such behavior can be understood by noting that both the real and imaginary parts of q possess the same functional dependence on λ_n (or $\tilde{\lambda}_n$), and thus

$$\frac{L_p}{\lambda_{\rm WGP}} \propto \frac{\Re{\rm e}\; q}{\Im{\rm m}\; q} \quad \Rightarrow \quad \text{independent of } \lambda_n \;, \tag{S39}$$

that is, $L_p/\lambda_{\rm WGP}$ is independent of λ_n ($\tilde{\lambda}_n$), and therefore this quantity is *universal* for both WGP, GGP, and flat-GPs, as the figure demonstrates. This characteristic is direct consequence of the "universal scaling law" stated by Eq. (S32).

Convergence of the solution via orthogonal polynomials expansion

Figure S4 clearly shows that the solution (for the first three modes) via orthogonal polynomials expansion technique converges fast with the number of polynomials used in the expansion for the electrostatic potential.

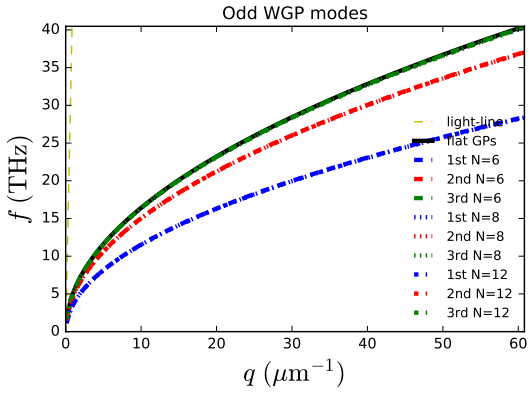

Figure S4: Same as Fig. S2, but using different values for the expansion truncation, N, to check the method's convergence.

2D Electric field distributions of WGP odd modes: further details

Further details on the 2D spatial distributions of the electric field akin to WGP odd modes.

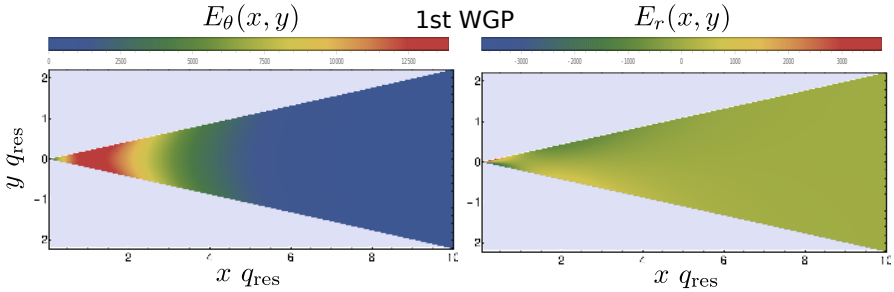

Figure S5: Both angular and radial components of the electric field (a.u.) akin to the first WGP odd mode. The parameters are the same as in Fig. S2. Only the region $-\varphi < \theta < \varphi$ is shown.

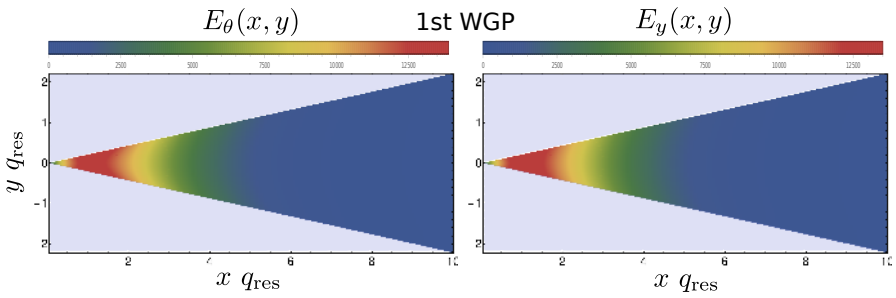

Figure S6: Comparison between the components of the electric field (a.u.) projected along $\hat{\boldsymbol{\theta}}$ (right panel) and $\hat{\mathbf{y}}$ (right panel). The parameters are the same as in Figs. S2 and S5. Note that $E_\theta(x,y) \simeq E_y(x,y)$. Only the region $-\varphi < \theta < \varphi$ is shown.

Dependence of FEM simulations on the rounding of the edge

Fully numerical simulations (with a local-response dielectric function) cannot handle infinitely sharp boundaries. For this reason, it was necessary to round (smooth) the otherwise sharp apex of the triangular wedge in our full-wave electrodynamic FEM simulations implemented in COMSOL Multiphysics commercial software. The influence of the radius of curvature (rounding) on the WGPs' wavevector is shown in Fig. S7. It can be observed from the figure that, as the radius of curvature (R_c) of the edge decreases, the value for the WGP propagation constant predicted by the simulations (dots) successively approaches the propagation constant given by our quasi-analytic model (dashed horizontal lines). However, if one takes the limit when $R_c \to 0$ the WGP wavevector eventually diverges to infinity. The effect is more dramatic for the fundamental mode than for the second order mode because the former possesses a smaller wavelength and therefore probes more deeply within the V-shape. In order to cope with this unavoidable nuisance we have chosen a *very small* radius of curvature, to mimic the (idealized) infinitely sharp interface considered here, but in such a way that it is not *too small* to produce divergences. Therefore, we have taken $R_c = 0.25$ nm in our FEM numerical simulations (corresponding to the third data point counting from the

left), a number within the ballpark of the 0.34 nm thickness of a monolayer of sp^2-hybridized carbon. Notice that values in the neighborhood of this value give similar results.

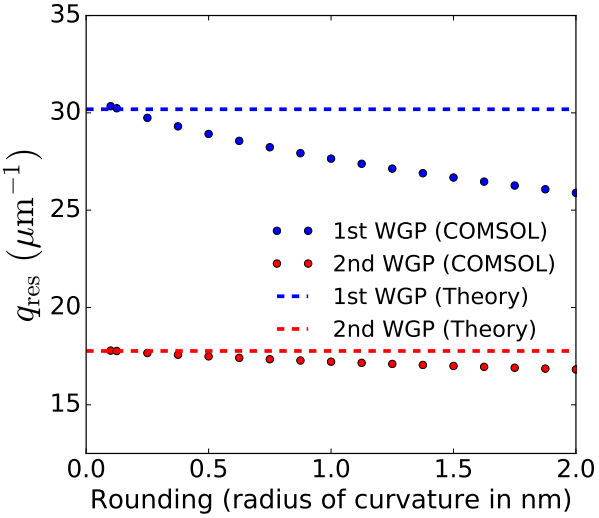

Figure S7: Guided graphene plasmon's wavevector, for $f = 20$ THz, as a function of the radius of curvature of the apex of the wedge. Note that the numerical solution—as expected—is sensitive to the parameter, since it cannot cope with infinitely sharp edges. The quasi-analytical model (horizontal dashed-lines), however, automatically handles the singularity at $r = 0$ by using the appropriate (analytic) Green's functions. Remaining parameters: $E_F = 0.4$ eV, $\epsilon_1 = 1$, $\epsilon_2 = 4$, and $2\varphi = 25°$.

Lastly, we note that in our COMSOL Multiphysics simulations the graphene sheet is modeled as a layer of (effective) finite thickness, $t_{\mathrm{eff}} = 1$ nm, with dielectric function $\epsilon_{\mathrm{g}}(\omega) = 1 + \frac{i\sigma_D(\omega)}{\omega\epsilon_0 t_{\mathrm{eff}}}$ where $\sigma_D(\omega)$ is the Drude conductivity of graphene.[7]

References

(1) Nikoshkinen, K. I.; Lindell, I. V. Image solution for Poisson's equation in wedge geometry. *IEEE Transactions on Antennas and Propagation* **1995**, *43*, 179–187.

(2) Scharstein, R. W. Mellin transform solution for the static line-source excitation of a dielectric wedge. *IEEE Transactions on Antennas and Propagation* **1993**, *41*, 1675–1679.

(3) Comment on the orthogonality of the Macdonald functions of imaginary order. *J. Math. Analysis and Applications* **2010**, *365*, 195 – 197.

(4) Dobrzynski, L.; Maradudin, A. A. Electrostatic Edge Modes in a Dielectric Wedge. *Phys. Rev. B* **1972**, *6*, 3810–3815.

(5) Wu, J.-W.; Hawrylak, P.; Eliasson, G.; Quinn, J.; Fetter, A. Magnetoplasma surface waves on the lateral surface of a semiconductor superlattice. *Solid State Communications* **1986**, *58*, 795–798.

(6) Wang, W.; Apell, P.; Kinaret, J. Edge plasmons in graphene nanostructures. *Phys. Rev. B* **2011**, *84*, 085423.

(7) Gonçalves, P. A. D.; Peres, N. M. R. *An Introduction to Graphene Plasmonics*; World Scientific, 2016.

(8) Abramowitz, M.; Stegun, I. A. *Handbook of Mathematical Functions: with Formulas, Graphs, and Mathematical Tables*; Dover: New York, 1965.

(9) Li, Z. Q.; Henriksen, E. A.; Jiang, Z.; Hao, Z.; Martin, M. C.; Kim, P.; Stormer, H. L.; Basov, D. N. Dirac charge dynamics in graphene by infrared spectroscopy. *Nature Phys.* **2008**, *4*, 532–535.